Catalysis Today 143 (2009) 315–325

Contents lists available at ScienceDirect

Catalysis Today

journal homepage: www.elsevier.com/locate/cattod

Surface anion vacancies on ceria: Quantum modelling of mutual interactions and oxygen adsorption

José C. Conesa *

Instituto de Catálisis y Petroleoquímica, CSIC, Marie Curie 2, Cantoblanco, 28049 Madrid, Spain

ARTICLE INFO

Article history:
Available online 3 January 2009

Keywords:
Cerium oxide
Modelling
DFT
Anion vacancies
Adsorbed oxygen
Redox catalyst

ABSTRACT

Quantum DFT + *U* calculations using periodic slab models are made to understand the characteristics of surface defects containing one, two or three anion vacancies at the CeO_2(1 1 1) surface. Several non-equivalent energy minima with different positions of localized Ce^{3+} ions can exist due to polaron-type distortions that influence the relative stability of Ce^{3+} in 6- and 7-fold coordinated sites. The calculated total energies do not confirm the tendency to vacancy association suggested by previous works. In the case of associated vacancies spontaneous outwards movement of one oxygen ion from a subsurface layer is observed. Oxygen adsorption on these defects leads to electron transfer to the O_2 molecule, forming peroxide species, except when only one electron is available in which case paramagnetic O_2^- species appear; the adsorption energies involved are computed and discussed. All these species appear asymmetrically coordinated to three surface Ce ions. The presence of excess electrons, as is the case when two or more vacancies associate, does not lead in general in these calculations to a barrierless complete reduction of the O_2 molecule, a process which would produce a pair of oxide ions; this is explained considering the relative energies of the orbitals involved. Thermal activation would be needed to complete this process.

1. Introduction

Cerium oxide is an important ingredient in redox catalysts active in chemical reactions such as combustion of organics, car exhaust gas cleaning, water gas shift (WGS), CO preferential oxidation (PROX), intermediate temperature solid oxide fuel cells or sulfur removal in FCC units [1]. Its high redox activity is to a large extent due to its ability to easily release and retake oxygen with concomitant change of cerium from the Ce^{4+} redox state to the Ce^{3+} state and back. In the process of reoxidation of the previously reduced solid, electrons (four in total) are transferred from Ce^{3+} ions to one incoming O_2 molecule to give in the end two oxide (O^{2-}) ions in lattice positions; paramagnetic O_2^- (superoxide) and diamagnetic O_2^{2-} (peroxide) species have been identified with EPR (for O_2^{2-}) [2–4] and vibrational [4–7] spectroscopies as products of the first stages of this process. It seems reasonable to assume that completing this reoxidation process will require having in close proximity the four Ce^{3+} ions that donate the electrons and the two anion vacancies that must accept the O^{2-} ions.

From this point of view it was interesting to observe, during an atomistic simulation work [8], that anion vacancies had apparently a tendency to associate on the (1 1 1) surface of CeO_2, that was predicted to be the most stable one, but not in the (1 1 0) surface, second in stability. This tendency to association had been suggested by EPR studies of nanocrystalline ceria samples activated at different temperatures [4], in which the change in EPR spectral parameters of O_2^- species (formed upon O_2 adsorption) that took place when rising the outgassing temperature to 573 K or higher was proposed to be due to anion vacancy clustering, and seemed to receive later additional support from STM and AFM measurements [9–13]. To help to clarify this issue, the present work presents a quantum simulation of the association of anion vacancies on the CeO_2(1 1 1) surface and of the adsorption of O_2 on them.

The simulation of the effect of reduction on the ceria surface has been already undertaken by other authors; a number of these are discussed in a recently appeared review [14]. Although some study has been carried out using Hartree–Fock-type approaches on finite cluster models [15–17] or periodic models [17], in almost all cases density functional theory (DFT) has been the basis of the calculations. In the last years it has become apparent that standard DFT, that was used in some earlier work [18,19], is inadequate to model bulk ceria or its surface when in the partially or fully reduced state [20] (and see also [21,22]), [23,24]. This is due to the fact that this level of theory has an unphysical, non-cancelled electron self-interaction that unduly promotes delocalization in

* Tel.: +34 915854766; fax: +34 915854760.
E-mail address: jcconesa@icp.csic.es.

0920-5861/$ – see front matter © 2008 Elsevier B.V. All rights reserved.
doi:10.1016/j.cattod.2008.11.005

the resulting electrons and predicts a metallic character of the 4f manifold, that contains excess electrons in its lower part. This problem has been solved in a number of more recent works by introducing a Hubbard-type correction term U (the DFT + U approach) [20,25–32] or, in other works, by using hybrid functionals that include some amount of Hartree–Fock exchange [17,23,24]; some self-interaction corrected calculations on Ce_2O_3 have been made as well [33]. In the present work, the DFT + U method is used; the hybrid functional method, although trying to correct the DFT adequacies in a more general (less *ad hoc*) way and consequently being more reliable in principle, gives incorrect results in some cases [34,35], and has furthermore a much higher computational cost if used with a plane wave basis set (that is much more adequate when accurate and well converged total energy values are desired, as is the case here). As will be apparent in the following, the results show significant effects of electron localization on Ce ions, atomic movements induced by vacancy association and electronic features of adsorbed dioxygen species that are related to the degree of electron transfer to them.

2. Methods and models

To represent the (1 1 1) surface, periodic slab models (Fig. 1), in which the slab surfaces are parallel to a (1 1 1) plane, were constructed from supercells of the bulk, non-reduced CeO_2 fluorite structure. In this latter the size of the primitive unit cell (3.8434 Å) was determined by relaxing it in a previous calculation of CeO_2 made within the same DFT + U theory level. In these slab models the unit cell axes a and b, parallel to the fluorite structure (1 1 1) plane and forming between them an angle of 120°, were derived from those of the cubic fluorite cell (a_f, b_f and c_f) through the operations $a = (a_f + b_f - 2c_f)$ and $b = (b_f + c_f - 2a_f)$, leading to an axis length of 13.314 Å ($2\sqrt{3}$ times that of the fluorite primitive cell axes), while the c axis, perpendicular to them, was long enough that the empty space between slabs was 11 Å (higher than the minimum value of 10 Å that has been reported as enough for convergence in this system [36]). These cell dimensions were kept fixed in all relaxations. Each atomic plane parallel to the slab has thus 12 atoms in this unit cell. It is expected that with this cell size the lateral interactions between the periodic images of the defects are kept small, or at most moderate, even for the largest of these defects, that consist of three neighbouring vacancies. In particular, the periodic dipoles associated with the defects studied were computed and the energy of interaction between them, once obtained, was found to contribute negligibly to the energy differences of interest in this work.

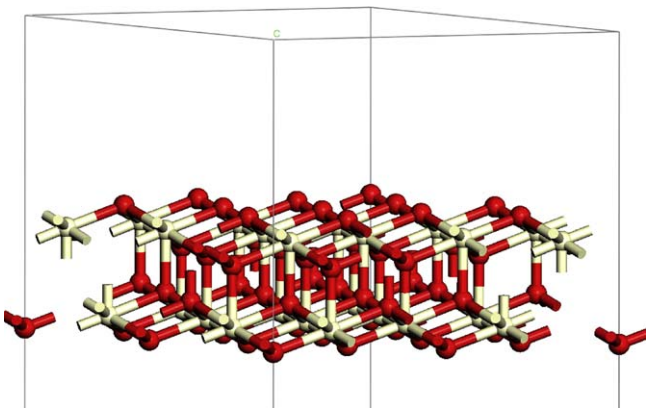

Fig. 1. Slab model used to represent the CeO_2(1 1 1) surface. Ce and O ions are coloured white and red, respectively. (For interpretation of the references to color in this figure legend, the reader is referred to the web version of the article.)

The thickness of the slab was chosen at a minimal value, with only six ion layers (four oxygen layers and two cerium layers), so that for the unreduced case the model contains 72 atoms. It is recognized that a larger slab thickness would be desirable to ensure that the results are not distorted by this factor (it has been reported that a slab with nine ion planes is adequate to ensure convergence in respect to thickness [37]); but in this work, that uses a large number of ions per layer, this had to be discarded to keep the problem computationally tractable. It is noted, in any case, that other works in the literature use the same slab thickness as here [38,39].

Defects (oxygen vacancies) were located only at the upper O plane of the slab, that will be taken here as origin of the z coordinate perpendicular to it; in this situation, the upper Ce plane has thus a coordinate $z = -0.785$ Å. Besides the perfect surface model containing no anion vacancy (designated with the label 0V), models containing one surface anion vacancy (labelled 1V) or two or three neighbouring surface anion vacancies (labelled 2V or 3V, respectively) were studied. In the latter 3V case the vacancies were arranged in a triangle, to enhance the effects of clustering. For this there are two possible main configurations; in one of them the centre of the vacancy triad is located above a Ce ion of the upper cation layer, in the other one it is above an interstitial empty site of that layer. The former configuration, in which the mentioned Ce ion has only four O neighbours, was verified to be much less stable; results derived from it will not be presented here. The situation in which only one excess electron is present was modelled by substituting by one La ion one of the Ce ions close to an isolated vacancy; this model will be designated 1VLa. Finally, structures obtained by adding to these models one O_2 molecule located on the surface will be labelled adding the suffix O_2 to the initial model name.

It was found that for each one of these vacancy defects different specific sub-configurations could appear (depending on the particular position of the ions in the unit cell of the model) in which the Ce ions which received excess electronic density (thus becoming Ce^{3+} ions) differed; these sub-configurations will be labelled where necessary by appending lowercase letters to the main labels mentioned above. The Ce^{3+} or Ce^{4+} nature of each Ce ion could be easily ascertained by examining in the output of the calculation the value of the total spin density integrated within the atomic spheres defined by the PAW potentials: in all the cases discussed here this value was either higher than 0.90 or lower than 0.05. It was also noted that in the first case the projection of the spin density on f-type spherical harmonics within these spheres accounted for the large majority of the mentioned value. Those two situations can be therefore safely ascribed to Ce^{3+} (with a $4f^1$ configuration) or Ce^{4+} ions. In some cases the mentioned sub-configurations could be obtained in the fully relaxed final structures only by previously displacing manually some O atoms towards or away from specific Ce ions so as to change the corresponding Ce–O distances by about 5% (the typical difference in Ce–O bond length observed in the calculations between Ce^{3+} and Ce^{4+} for any given coordination number). In part of these cases an initial displacement favouring specific locations of Ce^{3+} ions was achieved by making a previous calculation in which these locations were occupied by La atoms (as La^{3+} ions have typically ionic radii similar or larger than those of Ce^{3+}); the relaxed structures obtained in this way were then used as starting points for the definitive calculation involving only Ce and O atoms.

All calculations were made with the plane wave DFT code VASP (version 4.6) developed at the Institut für Material-physik of the Universität-Wien [40–43], representing the atomic cores with the PAW method [44,45] and using spin-polarized density functional theory at the GGA level according to the PBE functional [46]. The latter was supplemented with an effective Hubbard term

$U_{eff} = U - J$, of the rotationally invariant form proposed by Dudarev et al. [47], equal to 4.5 eV [23], applied to the Ce 4f levels, trying to correct the above mentioned excessive tendency of standard GGA to electron delocalization (it is noted here, however, that there is some debate about the best U value to use in these calculations [30–32,48]). The energy cut-off adopted for the plane wave representation of the wavefunctions was 375 eV, and the reciprocal space was sampled with a Γ-centred $6 \times 6 \times 1$ Monkhorst-Pack grid (such a dense grid was found to be necessary to have convergence of the energy differences in respect to the reciprocal space sampling). In all the calculations all atoms except for those at the bottom oxygen layer (that were kept fixed) were allowed to relax freely within the fixed cell dimensions, starting when necessary from atomic configurations having the symmetry partially broken in order to ensure that the system was not kept in a saddle point of the energy hypersurface. Partial density of states (DOS) curves were obtained through projection of the Kohn–Sham wavefunctions on spherical harmonics within the atomic spheres defined by the PAW potentials.

The self-consistent procedure determining the electron and spin density distribution for each geometry was always carried out leaving the total spin unconstrained and free to evolve as dictated by the aufbau principle; only an initial assignment of non-zero spin, in order to break the total spin symmetry, was applied to some Ce ions; but it was not uncommon that the ions chosen for this were not the same that appeared as Ce^{3+} ions in the final solution. In most cases the self-consistent calculation led to equal spin directions for all the Ce^{3+} ions present (i.e. to a ferromagnetic-type spin configuration); in other cases some of the Ce^{3+} ions appeared with spin orientation opposite to the other ones, suggesting an antiferromagnetic interaction. The strength of this interaction, related to the energy cost of changing the relative spin orientations, was not analysed (as could be done by forcing specific values of the total spin), but is expected to be rather small, since the 4f orbitals have typically very reduced overlap with neighbouring ones, and there are no itinerant electrons at hand to carry the spin polarization over several bond distances. The ferro or antiferromagnetic character of the vacancy defects, in any case, was not a main concern of this work, as it is unlikely to determine their stability or reactivity, and therefore the factors leading to one or other type of ordering were not studied.

3. Results and discussion

3.1. Single vacancy defects

The results obtained with models of 1V type, which predict always a full ionization of the anion vacancy, showed in agreement with previous works [25] that, even though the system has topological 3-fold symmetry, the latter spontaneously breaks so that the two extra electrons produced upon vacancy formation become localized in two Ce ions. It was also found that, depending on the exact geometry of the starting point, the structural relaxation could lead to different non-equivalent sub-configurations differing in the location of the Ce^{3+} ions; some of them are displayed in Fig. 2a–c. As said above, these are easily discernible in the calculation output through the values of the net spin population on cerium. As indicated in this figure, these final converged solutions had slightly different energies. Computing the total energies of the most stable of these solutions, the defect-free surface and an isolated O_2 molecule allows to obtain an energy balance for the vacancy formation process

$$Ce_{24}O_{48}\,(0V) \rightarrow Ce_{24}O_{47}\,(1V) + (1/2)O_2 \quad \Delta E = +2.45\,eV$$

Some calculation was also made in which one Ce ion was substituted by a La ion (Fig. 2, model 1VLa), in order to achieve a situation in which the presence of one vacancy was accompanied by only one excess electron (that also ended up localized in a Ce^{3+} ion). In this case an energy balance similar to the one above cannot of course be established.

It is interesting to note that the sub-configuration with lowest energy is not that which contains the Ce^{3+} ions located as immediate neighbours to the anion vacancy, i.e. in a 6-coordinated site (1Vd in Fig. 2), as could be anticipated on purely electrostatic grounds (since the ionized anion vacancy represents a net positive charge); the Ce^{3+} ions in the most stable sub-configuration are rather in 7-coordinated next-neighbour locations (sub-configuration 1Va in Fig. 2).

As already suggested in the literature when discussing the Tb_7O_{12} structure [49], which is derived from that of fluorite by ordering anion vacancies in it, the trivalent cations may prefer to sit in positions having higher coordination numbers. This may be due to the fact that lower coordination numbers, due to the decreased repulsion between anions, allow these to approach more the central atom, a situation which fits better with the lower ionic radius that is normally ascribed to the Ce^{4+} ion. Such preference of Ce^{3+} for larger coordination distances, and the better achievement of these when coordination numbers are large, is confirmed by an analysis of the coordination distances: in all the relaxed situations obtained here the average Ce–O distances for Ce^{3+} and Ce^{4+} ions that are not neighbours to the vacancy (i.e. are coordinated to seven oxygen ions) are 2.48 and 2.36 Å, respectively, while for Ce^{3+} and Ce^{4+} immediate to the vacancy (i.e. coordinated to six oxygen ions) these distances are 2.40 and 2.28 Å, respectively.

This association between the electron localized in a Ce^{3+} ion and the distortion of its immediate environment to achieve a higher Ce–O coordination distance (which stabilizes the 4f electron in that site) constitutes a polaronic effect. Anyway, the energy differences between these polaronic states are not large, which means that at ambient or higher temperatures a distribution of these situations can exist. The conversion between them will be probably fast, as it constitutes a process of polaron hopping that may have at the surface an activation energy lower than that of the bulk process (determined to be around 0.4 eV [50]).

The electronic structure of these situations can be visualized as well through the corresponding DOS plots. Fig. 3a shows the result for the perfect surface; the valence band, made mainly of O(2p) orbitals, and the upper manifold of unoccupied states, made mainly of Ce(4f) orbitals, appear separated by a gap of ≈2.2 eV. This value is lower than the experimental one (≈3.0 eV [51]); such underestimation of band gaps is typical of both standard DFT and DFT + U treatments. For models with one anion vacancy the results (Fig. 3b and c) show two spin-polarized levels in the band-gap, filled by two electrons and located ca. 0.8 eV below the main 4f manifold; the atom projected DOS shows that they correspond to the $4f^1$ states of the two Ce^{3+} ions present in these 1V-type models. Additional calculations (results not displayed here) show that, in agreement with previous works [20,26], this localization of electrons in individual Ce^{3+} ions, and the separation of these states from the rest of the 4f manifold (which agrees with experimental results), are not obtained when an effective Hubbard term U_{eff} is not added to the GGA functional. In these plots it can be observed that the energy of this DOS peak appearing in the band-gap slightly depends on whether the Ce^{3+} ion is located in a 6- or 7-fold coordinated site, the latter being preferred. This is in-line with the energy difference between sub-configurations 1Va and 1Vb in Fig. 2. In model 1VLa, built to simulate a situation with only one excess electron, the position of the latter in the band-gap (again corresponding to the $4f^1$ state of a Ce^{3+} ion) is similar to that found in the two-electron 1V models.

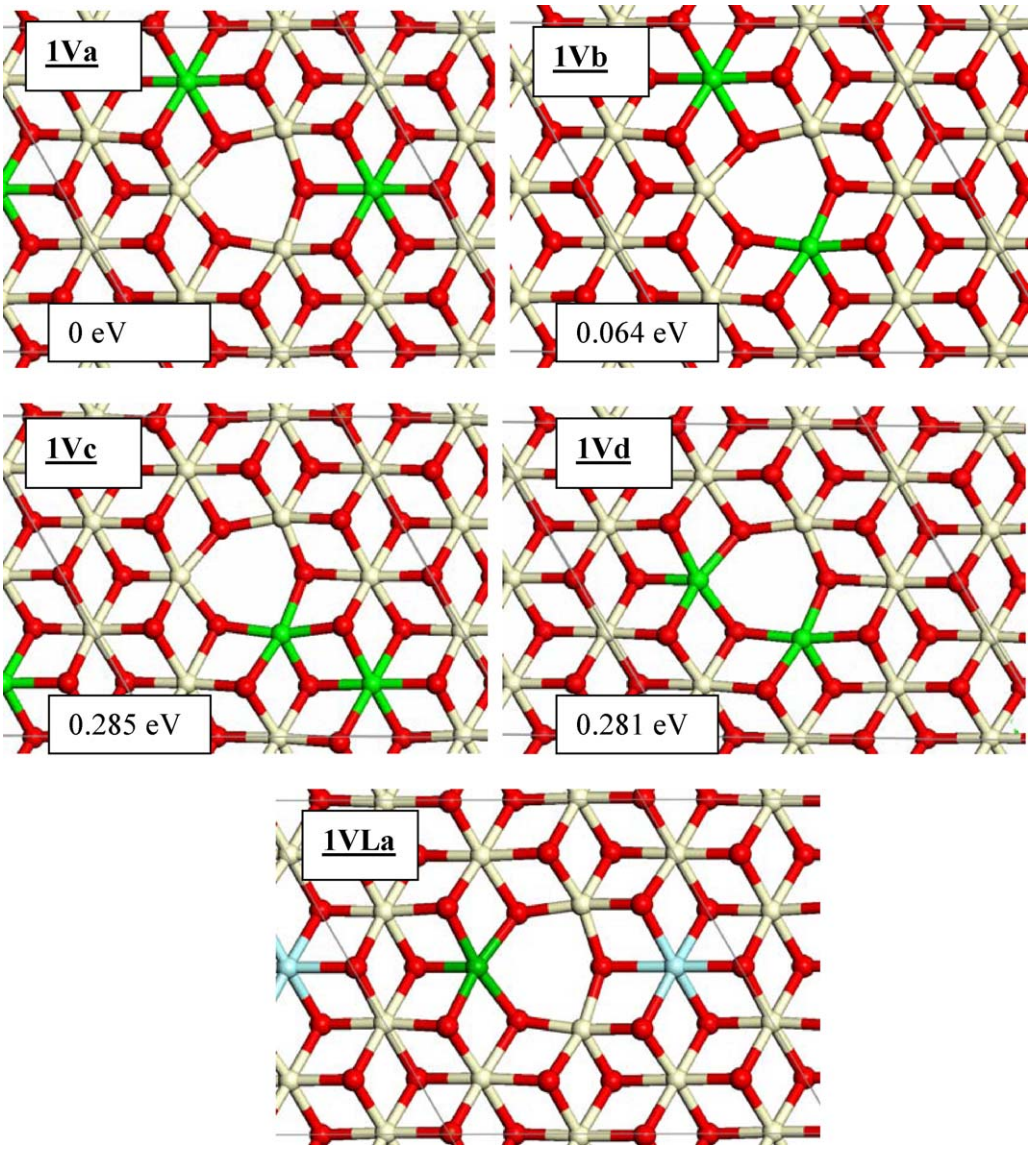

Fig. 2. Locations of Ce^{3+} ions (coloured green) for several of the energy-minimized structures (polaronic states) found after relaxation of single anion vacancy defects on a CeO_2(1 1 1) surface. For clarity only the three upper atomic layers are displayed. The drawing in the lower part corresponds to the model in which besides the vacancy a lanthanum atom (coloured light blue) is present substituting a Ce atom. The numbers inserted for the other drawings in the lower left corner indicate their energies (in eV) relative to that of the lowest one (1Va). (For interpretation of the references to color in this figure legend, the reader is referred to the web version of the article.)

3.2. Vacancy pairs

A complex of two vacancies located together was then simulated. In this case four excess electrons are present that become localized to give four Ce^{3+} ions, implying eventually breaking of the maximum topological symmetry of the defect. Again polaronic effects occur, and different inequivalent local energy minima can result depending on the precise initial position of the atoms. The number of possible sub-configurations is rather high, and only some of them have been characterized in the calculations; several of these can be seen in Fig. 4. A clear rule about the preference or not of Ce^{3+} ions for sites immediate to the vacancy cannot be observed, contrarily to what was observed for the single vacancy defects. Maybe the more important and asymmetric structure distortion caused by the close location of two vacancies outweighs the factors that govern the optimal Ce^{3+} location in the case of the single vacancy. Still, one can observe now that in all of the local minima obtained one of the Ce^{3+} ions is found at the position that is nearest neighbour to both vacancies. Apart from this, several inequivalent situations appear within a close energy interval, and as in the case of a single vacancy one can foresee that fast exchange among them may occur at finite temperatures. One relevant observation is that, considering the lowest energy sub-configurations found for each case, the following energy balance can be obtained:

$$2 * 1V \rightarrow 0V + 2V \quad \Delta E = +0.34\,eV \tag{1}$$

This means that the association of vacancies in pairs is energetically uphill, i.e. would not be favoured on this surface. This result disagrees with the previous atomistic calculation [8] which predicted for the same process a net energy change of $\Delta E = -0.52$ eV. The present result also would not allow to explain some STM observations in the literature [9,11,13] which claim that surface anion vacancies on CeO_2(1 1 1) tend to form triads or to associate in strings. Such disagreement between DFT and atomistic calculations when predicting the relative stability of different atomic orderings within the same fluorite structure has been found

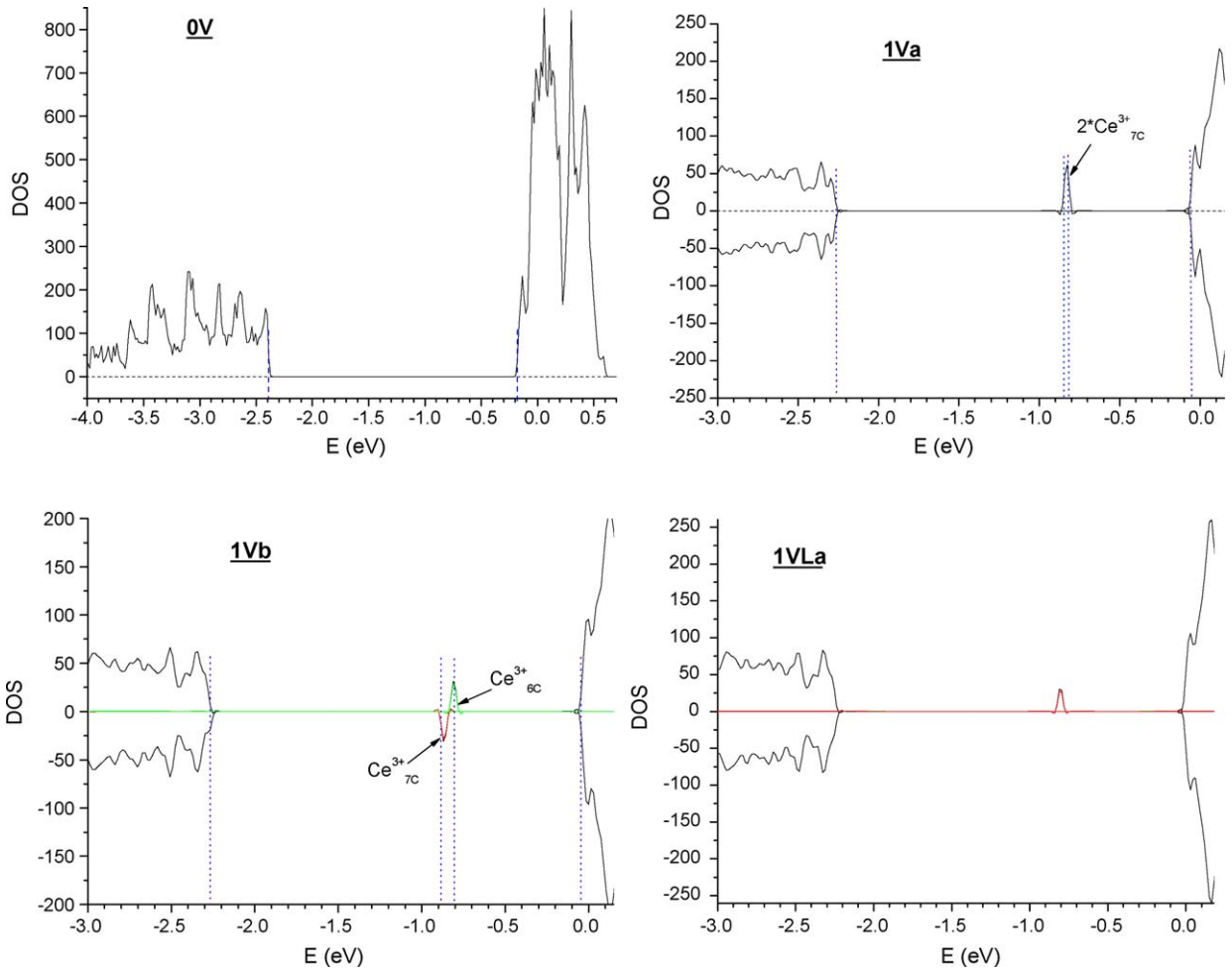

Fig. 3. Density of states (DOS) plots obtained for the models of the perfect CeO_2(1 1 1) surface (given in Fig. 1) and of several of the single-vacancy defects mentioned in Fig. 2. In parts (b)–(d) majority and minority spin contributions are plotted respectively in the positive and negatives sides of the plots. Coloured curves indicate partial DOS projected on specific atoms of the structure. In these and other DOS plots vertical blue lines are given as guide to the eye where considered helpful to better appreciate positions and separations of several features in the plots. All in-gap features marked as Ce^{3+} are electron-filled, the large 4f manifold above them is empty. (For interpretation of the references to color in this figure legend, the reader is referred to the web version of the article.)

already in studies on ceria–zirconia systems [52]. In principle one would think that DFT calculations are more reliable than atomistic ones; in this respect it must be noted that atomistic calculations use formal charges, and therefore exaggerate the magnitude of the Coulomb interactions. It should be remembered however that DFT does not reproduce dispersion (London) interactions, which were included in the atomistic calculations through r^{-6} terms and could be significant in this type of oxides in which the polarizability of both anions and cations is high. It would be interesting to assess the influence of such dispersion interactions on the final energy balance, but this lies outside the scope of the present work.

Concerning the atomic positions that result after relaxation, the observed Ce–O average distances for 6- and 7-coordinated Ce^{3+} and Ce^{4+} ions are similar to those reported above for single vacancies, while for the 5-coordinated Ce^{3+} ions they are around 2.31 Å. One interesting result of these calculations is that the sub-surface O atom that is nearest neighbour to both surface vacancies is pushed outwards, going through the outer Ce plane and ending with a z coordinate $z = -0.60$ Å, i.e. 0.19 Å above this Ce plane (see Fig. 4). In so doing, this O atom breaks the bond that it had with a second-layer Ce ion. The driving force for this displacement is probably connected with the surface electric dipole that appears upon vacancy formation due to the net flow of electronic density from the outer O plane to the Ce plane immediately below; when a vacancy pair is made the local dipole increases, producing an increase in electrostatic energy that can be partially alleviated by displacing outwards some negative charge. This can be achieved with the mentioned movement of the sub-surface oxygen ion. An alternative way of describing the effect is to consider that the displacement helps to achieve a less uneven distribution of ligands around the Ce ions which are immediate neighbours to the vacancy pair. It would be interesting to verify whether such displaced oxygen could display a distinct chemical reactivity in surface processes.

Examination of DOS curves (Fig. 5) allows to assess the nature of the electronic levels present in this vacancy pair situation. It can be seen that again some occupied 4f levels appear in the band-gap, well separated from the manifold of empty 4f levels. The positions of these occupied levels in the gap depend again somewhat on the coordination of the Ce^{3+} ions to which they belong, but in a more complex way than what was observed for the single vacancy defects; in fact, the level does not always appear to be lower for 7-coordinated sites than for the other sites. The stronger structural distortions caused by this larger and less symmetric defect is probably at the origin of these variations. The result is a larger overall width of the in-gap feature. It would be interesting to check if experimental photoelectron spectra can detect this increase in width of the in-gap features when the concentration of surface vacancies increases. It is also noted in the DOS plots that a detached state appears slightly above the valence band. This seems to be

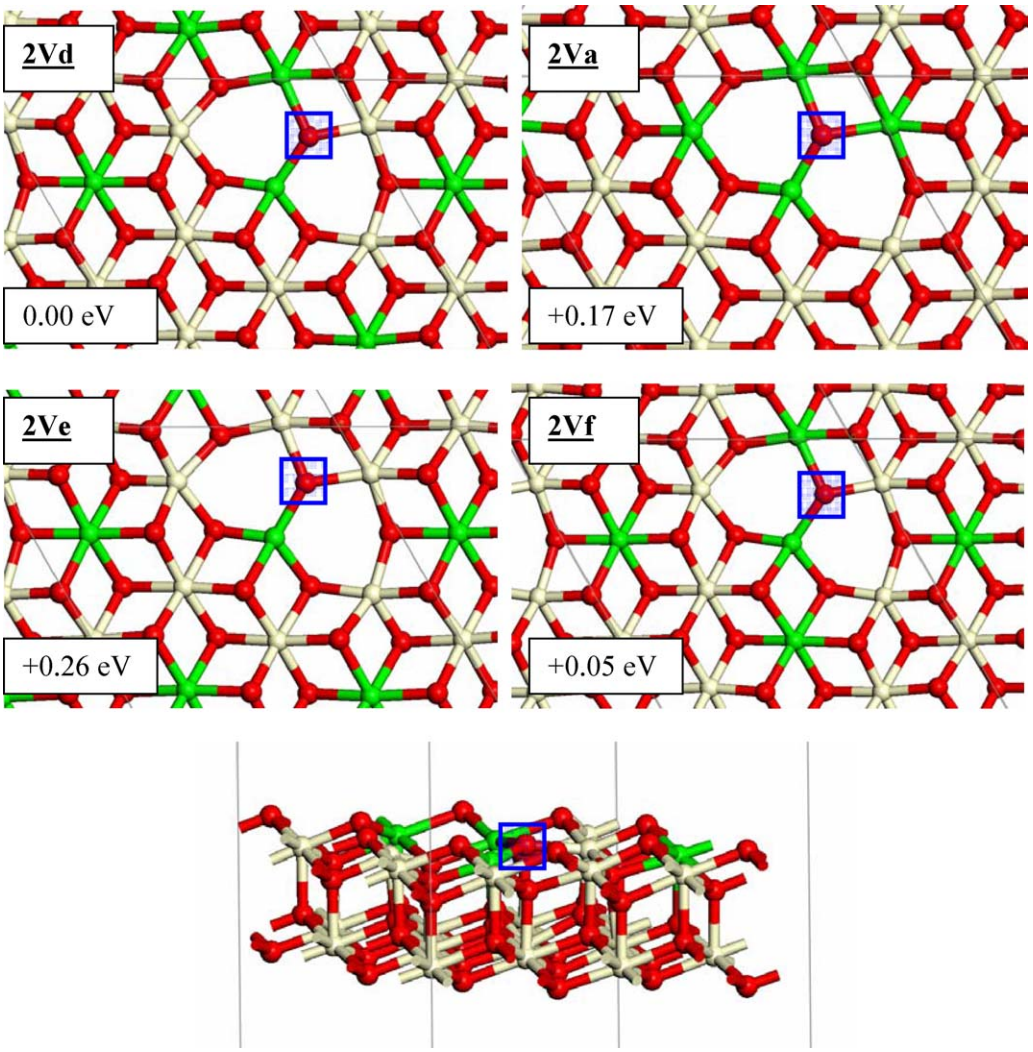

Fig. 4. Four upper drawings: locations of Ce^{3+} ions for several of the energy-minimized structures found upon relaxation of pairs of anion vacancies on a CeO_2(1 1 1) surface. Coding and meaning of numbers is as in Fig. 2. Lower drawing: perspective side view of structure 2Vd, to better appreciate the sub-surface oxygen ion that is pushed outwards in this type of defect. This oxygen is marked with a blue square in all the drawings. (For interpretation of the references to color in this figure legend, the reader is referred to the web version of the article.)

related to the oxygen ion that was pushed up from the sub-surface layer, since the contribution of this ion to the density of states of this feature is found to be significant, and again suggests a possibly higher reactivity of it.

3.3. Vacancy triads

An even larger number of possible sub-configurations can appear due to the different possible distributions of the six

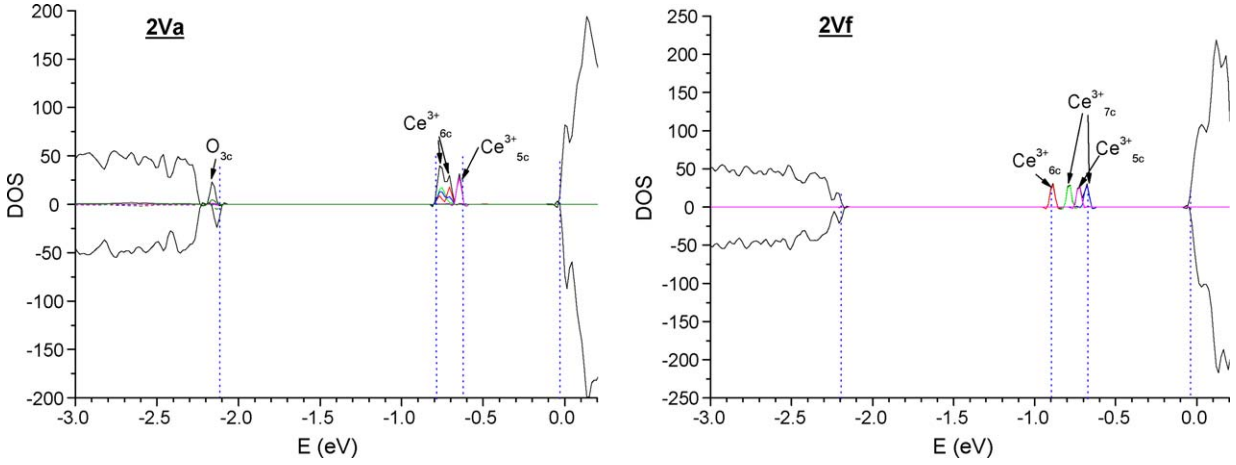

Fig. 5. Density of states plots obtained for some of the vacancy pair sub-configurations displayed in Fig. 4.

electrons generated upon formation of three vacancies. As shown in Fig. 6, where several of them are displayed, with the unit cell used here it would be possible to distribute all these electrons in Ce ions that are not nearest neighbour to any of the three vacancies if these are arranged in a cluster; the six electrons could also be distributed in the opposite way, i.e. with all of them on Ce ions neighbour to the vacancies. In the cases in which 5-coordinated Ce^{4+} ions appear the average Ce–O distance around them is 2.22 Å. None of these two situations appears to have the lowest energy, as seen in that figure; but it can be remarked that now the sub-configuration with all Ce^{3+} ions in 7-coordinated sites (3Vc in Fig. 6) has the highest energy among those examined, evidencing that the preference of Ce^{3+} for one site or another depends on the whole set of interactions that enter into play. Consequently a clear rule for preferences in the location of Ce^{3+} ions is difficult to find, although a preference for occupying with Ce^{3+} any 5-coordinated Ce ions, already noticed for vacancy pairs, seems to be present here also. In any case, again several closely located energy minima are found, so that under real finite temperature conditions the coexistence of a number of sub-configurations, and fast exchange between them, cannot be excluded. Note that, with these large vacancy complexes, even using a 12-fold surface supercell as done here it is not possible to discard some effect of interactions between these large defects that could influence the obtained energy values.

The formation of these vacancy triads is again predicted by the calculations to be unfavourable, as shown by the total energy balance of the following process:

$$1V + 2V \rightarrow 0V + 3V \quad \Delta E = +0.34\,eV \tag{2}$$

In these triads the outwards displacement of one of the sub-surface O ions, in particular that located at the centre of the defect, is observed also (Fig. 6); its z coordinate is in this case higher, typically around −0.15 Å, i.e. the displacement is much larger than for the two-vacancy complex. The explanation of this effect can be given, as said above, on the basis of a compensation of the surface dipole (that is larger in a three-vacancy defect) and/or of a tendency to make more regular the coordination environment of the Ce ions neighbour to the defect.

The nature of the electronic states that appear upon formation of this vacancy complex can be analyzed through the DOS curves; some of them, corresponding to a few significant sub-configurations, are displayed in Fig. 7. A number of distinct in-gap levels due to discrete Ce $4f^1$ states are observed; in general, those associated with 5-coordinated Ce ions appear lowest in energy, while those of 6- and 7-coordinated Ce ions are rather closer, with some tendency to have lower energy in the latter case. The result is that a large overall width appears when there is a heterogeneity of situations, while if all Ce^{3+} ions lie in the same type of coordination (sub-configuration 3Vc) the width is much smaller. Again, this could perhaps be experimentally examined with photoelectron spectroscopies. It is interesting to observe that the average position of these levels (except in the case of the less stable sub-configuration 3Vc) is located approximately 1.5 eV above the valence band edge, i.e. at nearly the same energy as for single vacancies (see Fig. 3); the highest $4f^1$ levels observed are at most only some 0.15 eV above this position. This suggests that although this situation corresponds to a more extensively reduced state of the surface (within the limits studied here), its redox potential is nearly the same, i.e. the excess electrons in it will not be transferred to external molecules much more easily than from a less reduced state. On the other hand, a detached state above the valence band is not observed now, in spite of the fact that an outwards-displaced O ion also appears in all these cases. Maybe the local asymmetry around this ion is a determinant factor for producing this less stable valence band state.

3.4. Anion vacancy-adsorbed oxygen species

The calculations show that after interaction of one oxygen molecule with a single vacancy all Ce ions are in the Ce^{4+} formal redox state and the total spin density is zero everywhere, implying that two electrons are transferred to the molecule (whether this happens in one or two steps is of no concern here) to form a

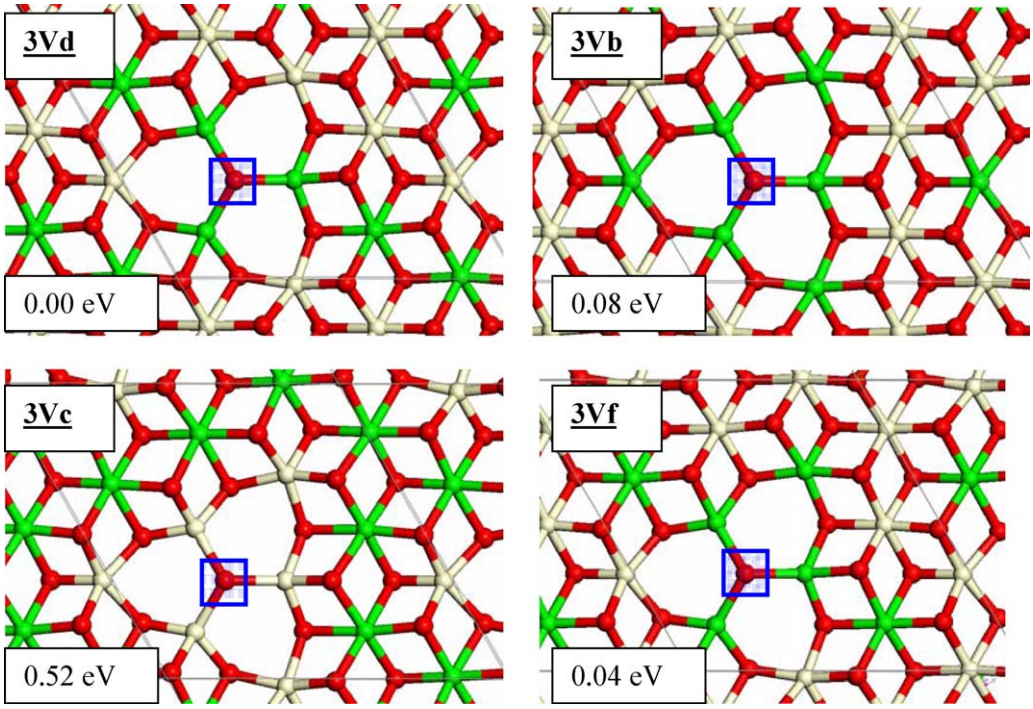

Fig. 6. Locations of Ce^{3+} ions for several of the energy-minimized structures found upon relaxation of a triad of anion vacancies on a CeO_2(1 1 1) surface. Coding and meaning of numbers is as in Fig. 4. (For interpretation of the references to color in this figure legend, the reader is referred to the web version of the article.)

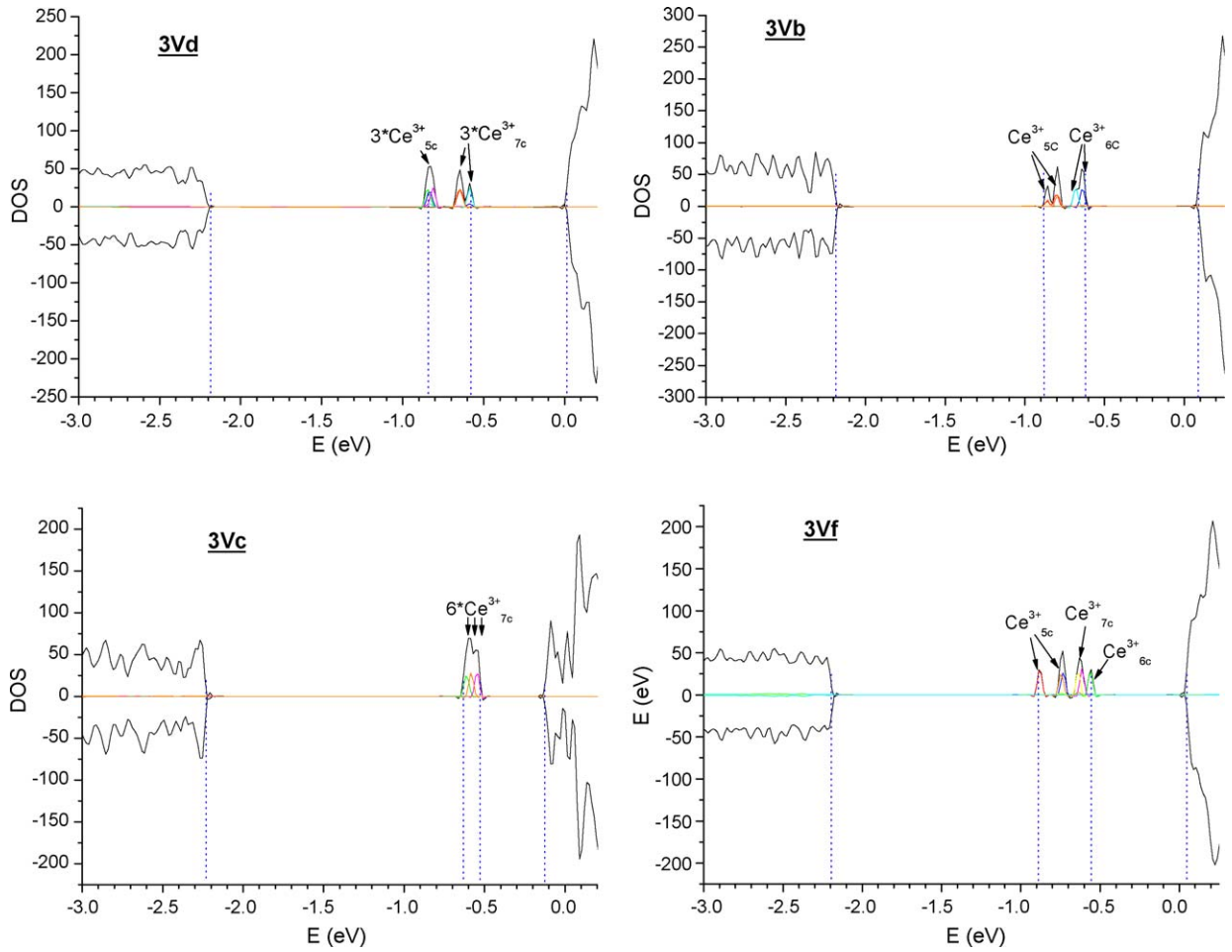

Fig. 7. Density of states plots obtained for some of the vacancy triad sub-configurations displayed in Fig. 6.

diamagnetic O_2^{2-} (peroxide) species; in the latter the interatomic distance is d(O–O) = 1.44 Å (Fig. 8, model 1VO_2). As seen in the figure, the O_2^{2-} ion is coordinated asymmetrically, with its bond oriented forming an angle of 36° with the surface plane. One of the two O atoms in it lies close to the vacancy centre, but slightly above the outer O atoms plane (its z coordinate is 0.14 Å) and somewhat displaced towards two of the Ce ions nearby so that its distance to them is around 2.42 Å, while the other O atom, significantly outside the upper O plane of the surface, interacts with the third Ce ion near the adsorption site with a distance d(O–Ce) = 2.30 Å. The adsorption energy is computed to be 2.10 eV if starting from the vacancy sub-configuration of lowest energy (1Va, displayed in Fig. 2). All these observations agree with the results reported in previous work [53], although in the latter the computed adsorption energy was 1.76 eV; this difference may be related to the different size of the unit cell used there (four atoms per atomic plane and nine atomic planes in the slab, with three planes in fixed atomic positions) as well as the different calculation method (use of ultrasoft pseudopotentials and U parameter referred to Wannier-type functions rather than to atomic orbitals).

A superoxide species adsorbed on a single surface vacancy site appears when the initial vacancy model is prepared in such a way that it contains only one excess electron (in form of Ce^{3+}), as is the case for model 1VLa mentioned above. In this case, after O_2 adsorption no Ce^{3+} ion remains, implying that the electron is transferred to the molecule; the adsorption energy computed for this process is 1.40 eV. The resulting O_2^- species has an overall geometry relatively similar to that of the peroxide species described above. It lies in somewhat outer position so that its distances to Ce ions are larger: one of its O atoms, located above the outer oxygen plane (its z coordinate is +0.61 Å), interacts mainly with two of the Ce ions neighbour to the vacancy, the O–Ce distances being now respectively 2.58–2.75 Å, while the other O atom interacts with the third Ce ion at a distance of 2.53 Å. These longer distances reflect probably the smaller Coulomb attraction between the Ce ions and the less charged dioxygen moiety. The length of the O–O bond (again oblique to the surface plane, forming with it an angle of 27.4°) is now 1.34 Å, shorter than that of the O_2^{2-} species as expected for a superoxide entity.

Close examination of the electron spin density distribution in this paramagnetic state shows that it is centred largely on the O_2^- species; the projections of this spin density on the individual atoms (the total of which amounts to 0.82 electrons; the rest is not captured by the projection method) indicate overall spin populations of 0.325 and 0.45 electrons for the inner and outer O atoms respectively. A large fraction of the rest lies on the Ce atoms (mainly on their 4f orbitals) that interact with these O atoms, since the spin populations observed on them are respectively 0.017 electrons (for the pair of Ce atoms in contact with the innermost oxygen) and 0.01 electrons (for the Ce atom in contact with the outermost oxygen). This presence of some spin density on the Ce 4f orbitals agrees with the significant degree of covalent interaction between Ce and superoxide species adsorbed on it that has been invoked [2–4,54] to explain the unusual EPR g values of O_2^-–Ce^{4+} species (in particular for the g_x parameter, that in contrast with most adsorbed superoxide radicals is in this case

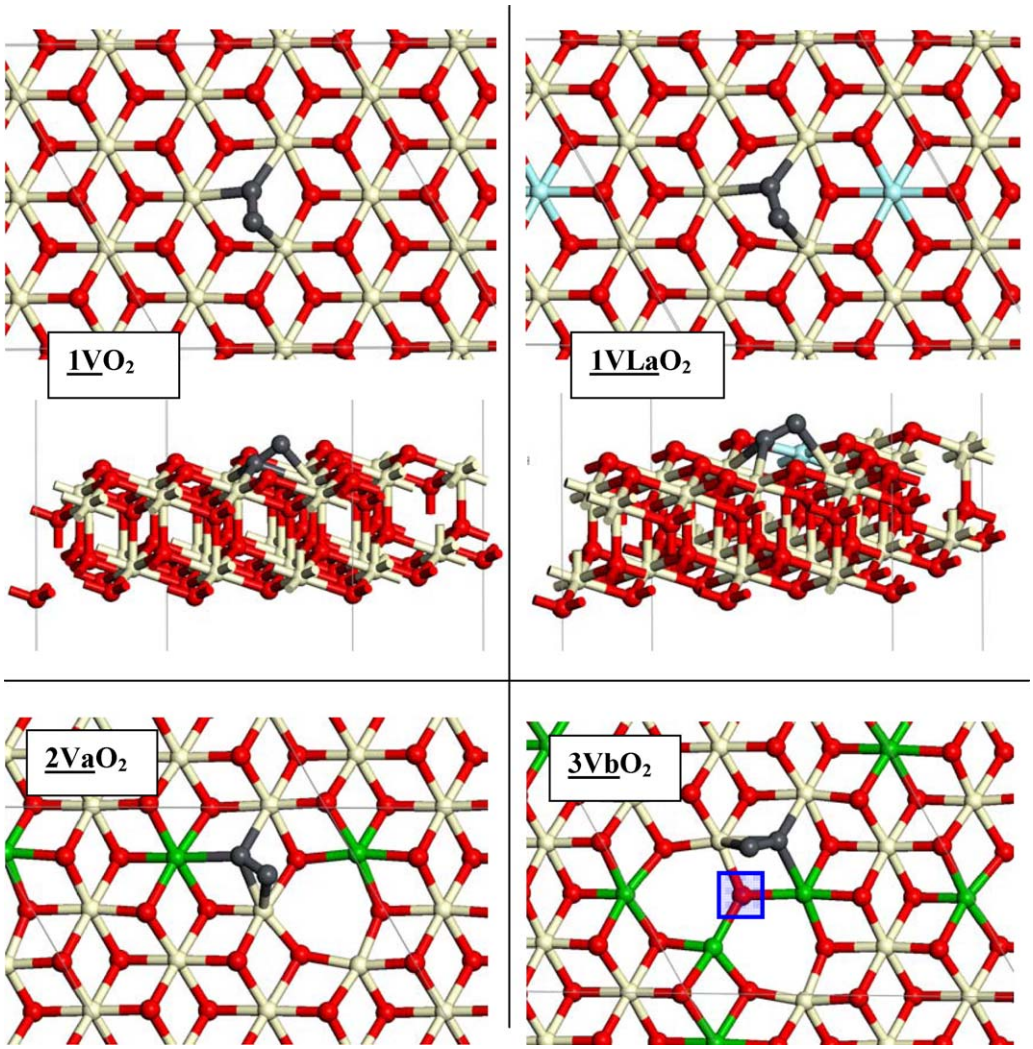

Fig. 8. Structures of dioxygen species adsorbed on several of the surface anion vacancy centres. $1VLaO_2$ is a superoxide (O_2^-) species, the others are peroxide (O_2^{2-}) species. *Z*-direction and perspective side views are displayed for the cases of adsorption on single vacancy configurations. The dioxygen species are coloured dark grey; for other atoms, colour coding is as in previous figures. In model $3VbO_2$ a blue square marks the O ion coming from the sub-surface plane that still remains near the outer Ce ion plane. (For interpretation of the references to color in this figure legend, the reader is referred to the web version of the article.)

significantly higher than the free electron value g_e). It should be noted on the other hand that for the latter species, when formed by adsorption of O_2 on slightly reduced high surface area ceria, the hyperfine structure observed when using ^{17}O-labeled O_2 [4] indicates that the two O atoms in it are equivalent at least in the time scale of the EPR measurement at 77 K or higher temperature. This means that either the dioxygen moiety has a fast oscillation movement which effectively averages the environment of its two extremes, or that the complex described here formed on the anion vacancy at the (1 1 1) surface of CeO_2 is not an appropriate model for the species observed by EPR. This complex could be, on the contrary, a good model for the main species formed on surfaces activated at higher temperature (up to 773 K), in which the same isotope labelling does evidence the non-equivalence of both oxygen atoms [4].

The examination of the DOS plots obtained for the two adsorbed states described above (Fig. 9) shows the presence of discrete levels within the band-gap due to the dioxygen moiety. For the peroxide case $1VO_2$ (that is fully diamagnetic, so that the total, spin-unpolarized result is shown) two doubly occupied levels appear, corresponding to the two antibonding π^* orbitals of the peroxide ion; they are split by approximately 0.22 eV due to the interaction with the surface. The fully occupied bonding π orbitals are clearly much lower in energy. On the contrary, the antibonding σ^* orbital must lie at much higher energy, as it is not discerned in the atom-projected curves.

For the superoxide case (model $1VLaO_2$) the antibonding π^* orbitals can again be discerned in the DOS plots. Due to the exchange interactions in this spin-polarized system the minority spin components of these levels (the upper of which is empty, as expected) appear at higher energy than the majority spin ones; in fact the lower of these latter overlaps the valence band and hybridizes with it leading to a large broadening of its features. The splitting between the two π^* levels (in the minority spin branch) is 0.26 eV, i.e. similar to that found for the peroxide case discussed above; this reflects the similarity in the type of cations that stabilize these species. Note that the energy at which the mentioned empty level appears is much lower than that of the $4f^1$ levels that appear in the gap when Ce^{3+} is present. It is thus not surprising that, as shown in this work, whenever two electrons are associated to a vacancy defect the adsorption of O_2 leads to full transfer of both electrons and the formation of peroxide rather than of superoxide species. This supports the above made suggestion that the surface defects that experimentally produce

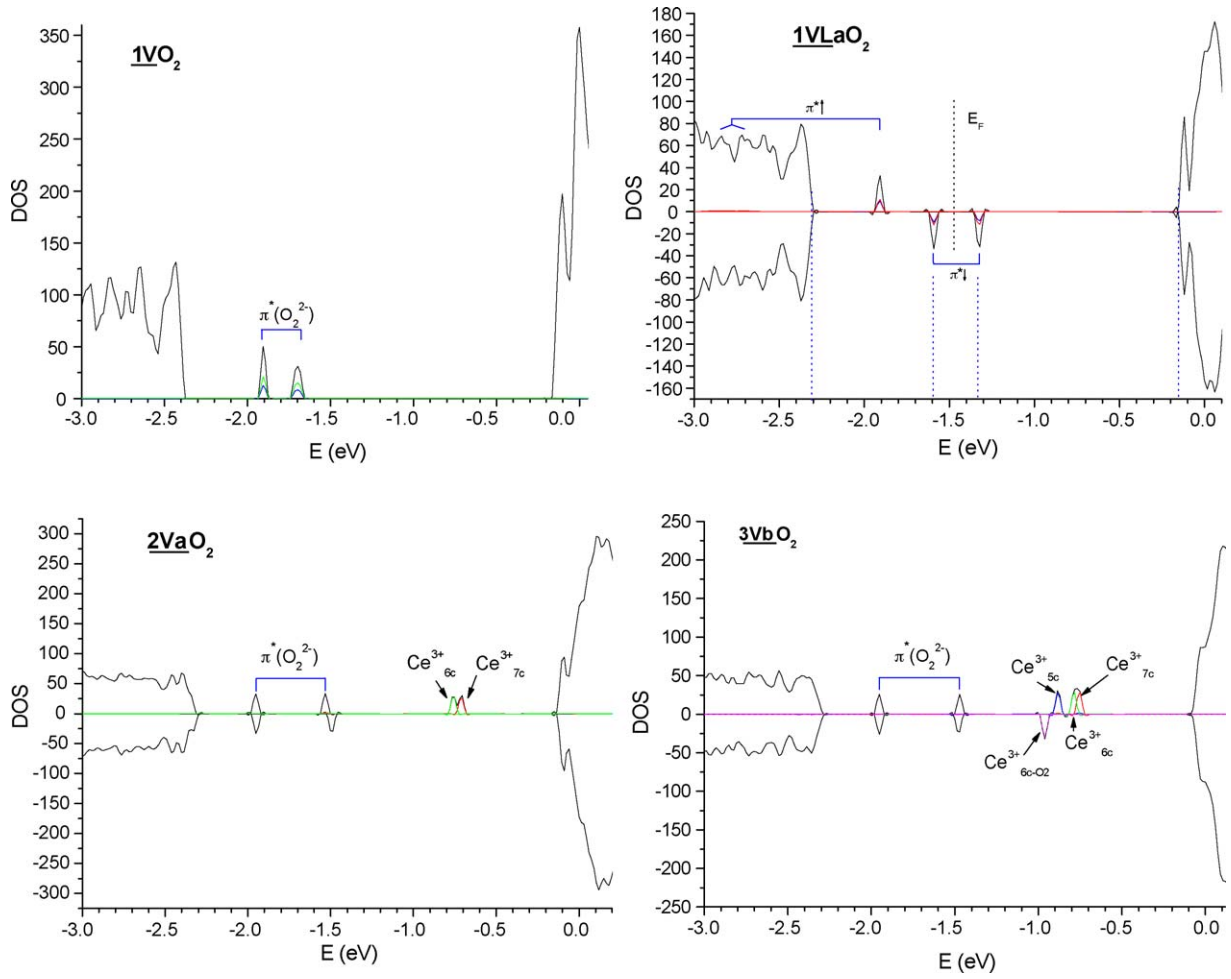

Fig. 9. Density of states plots obtained for the adsorbed dioxygen species displayed in Fig. 8. In the case of model $1VLaO_2$ the vertical dotted line between the two minority spin π^* features marks the separation between filled and empty levels.

EPR-detectable O_2^- species when O_2 is adsorbed on activated high surface area CeO_2 [see Ref. [4] and references therein] are not modelled adequately by the single or multiple vacancy structures on CeO_2(1 1 1) that are studied here. Maybe those species form on other surface planes, or on edge or kink irregularities present on the ceria nanoparticles.

The adsorption of O_2 on vacancy pairs and triads was studied also. It was found that in general peroxide species appeared, accompanied by respectively two and four Ce^{3+} ions (i.e. two electrons were transferred to the adsorbed molecule). Only in one case (for one of the vacancy pair sub-configurations) the adsorbed species evolved with breaking of the O–O bond and full reoxidation of the surface defect to the 0V structure; this behaviour appeared in this latter case probably due to some specific characteristic of the initial atomic arrangement, with the O_2 molecule above the defect, chosen in the energy minimization. In all the remaining cases (see Fig. 8 for a couple of typical examples) peroxide species rather similar to that found upon adsorption on a single vacancy (i.e. to the $1VO_2$ case) were found, occupying one of the initially existing vacancies. The energies of adsorption on the 2V and 3V complexes, computed from the lowest sub-configurations in each case, are 2.34 and 2.24 eV respectively, somewhat higher than on the single vacancy; this can be due to the higher interaction with the neighbour Ce ions that is discussed below. The *z* coordinates (in respect to the outer plane of O ions) of the O atoms closest to the initial vacancy centre are approximately +0.24 Å for both models $2VaO_2$ and $3VbO_2$. No spontaneous further transfer of electrons from Ce^{3+} ions to the adsorbed species is observed in these simulations, which is probably related to the fact that the σ^* orbital of the molecule, to which the electrons of the $4f^1$ orbitals would have to be transferred, lies higher in energy than these latter as shown above. Presumably, only by elongating the O–O bond (as may happen during thermal activation of molecular vibrations) can the σ^* orbital be lowered in energy to the extent necessary to make possible that transfer.

One noticeable difference is that the two O atoms of the adsorbed species interact now more strongly than in the $1VO_2$ case with one of the Ce ions closest to the initial vacancy, in particular with a Ce ion that initially (before O_2 adsorption) was 5-coordinated and in the Ce^{3+} state, and has now become a Ce^{4+} ion. The average distances from this Ce ion to the two O atoms of the peroxide species are now 2.47 and 2.27 Å (for model $2VaO_2$) or 2.50 and 2.27 Å (for model $3VbO_2$), while in the $1VO_2$ case they were 2.62 and 2.30 Å. Conversely the distance from the O atom near the vacancy centre to the other two Ce ions increases; the weakened interaction of this O atom with these Ce ions may explain why its *z* coordinate is higher than in the $1VO_2$ case. Thus, although the extent of electron transfer to the adsorbed species on associated vacancies is very similar to that found on the single vacancy (as shown by the population analysis obtained in the results; data not shown), this species can probably be considered to be more activated in the former case. Finally it is worth noting that the sub-surface O ion that had been pushed outwards on formation of the vacancy pair has returned to its sub-surface plane

after O_2 adsorption and formation of the peroxide species (case $2VaO_2$), as expected considering the partial return of the electron density towards the outer plane, while for model $3VbO_2$, where two neighbour vacancies still exist, this has occurred only partially, and this O ion remains just 0.28 Å below the outer Ce ion plane.

The examination of the DOS plots obtained for the species adsorbed on vacancy pairs or triads (Fig. 9) shows again the peaks above the valence band that are due to the π^* orbitals of the peroxide ion, and clearly above them the $4f^1$ levels of the remaining Ce^{3+} ions. The splitting between the two π^* orbitals is now around 0.45 eV, significantly larger than that found after adsorption over the single vacancy; this agrees with the above-mentioned higher interaction between the O_2^{2-} species and one of the neighbouring Ce^{4+} ions. The manifold of Ce $4f^1$ states is wider in the $3VbO_2$ case, as corresponds to a more complex and irregular defect.

4. Conclusions

The atomic and electronic structures and the energetics of surface anion vacancy complexes formed at CeO_2(1 1 1) surface, and of dioxygen species adsorbed on them, have been analyzed with quantum calculations at the DFT + U level of theory. The possible existence of a number of non-equivalent different (meta)stable locations for the resulting Ce^{3+} ions, accompanied and stabilized by local coordination distortions (polaronic effect), is evidenced by the calculations. Highly unsaturated (5-coordinated) Ce ions stabilize more markedly the extra electrons, but the preference of these for 6- or 7-coordinated Ce ions is less clear and may depend on the interplay of different structural distortions. A tendency to association of these vacancies, suggested by previous works, is not justified by the present results, but it should be recalled that the theory level used does not include dispersion interactions, that might be significant in this type of system which has highly polarizable ions. Outwards displacement of sub-surface O ions is shown to occur upon association of surface anion vacancies, to compensate for the increased surface electric dipole.

Adsorption of O_2 on these surface defects produces in general diamagnetic peroxide (O_2^{2-}) species due to transfer of two electrons to the molecule, except when only one electron is available in which case paramagnetic superoxide (O_2^-) species appear. This is explained on the basis of the relative energies of the π^* orbitals of the dioxygen species and the $4f^1$ levels of cerium, clearly visualized with density of states plots. All these diatomic species are stabilized by interaction with three Ce ions in asymmetric configurations; the equivalence between the two O atoms that has been experimentally observed with EPR spectroscopy in the case of some superoxide radicals adsorbed on ceria requires therefore some other explanation, based e.g. on molecular movement and/or different surface vacancy models. A higher degree of electron transfer, that would be necessary for O–O bond breaking, is not seen to occur here spontaneously; this is ascribed to the rather high energy of the dioxygen σ^* orbital that must receive additional electron density to complete the process. The activation energy for this bond breaking remains to be determined, and is the subject of an ongoing study.

Note added in proof

Very recent work (M. Veronica Ganduglia-Pirovano, Juarez L.F. Da Silva and Joachim Sauer, Phys. Rev. Lett. in press) reports as well that Ce(3+) may stabilize in different non-equivalent locations around an anion vacancy at the ceria(1 1 1) surface, and that the most stable location is a non-nerarest neighbour site.

Acknowledgements

Financial support from the Spanish National Research Plan (project CTQ2006-15600/BQU) and the possibility of using computing time at the MareNostrum and Finis Terrae parallel computers provided respectively by the BSC and CESGA computing centres are thankfully acknowledged. Thanks are given also to Dr. V. Ganduglia-Pirovano for useful discussions and hints concerning the polaronic effects.

References

[1] A. Trovarelli (Ed.), Catalysis by Ceria and Ceria-Containing Materials (Catalytic Science Series), World Scientific-Imperial College Press, London, 2002.
[2] M. Che, J.F.J. Kibblewhite, A.J. Tench, M. Dufaux, C. Naccache, J. Chem. Soc., Faraday Trans. I 69 (1973) 857.
[3] L. Mendelovici, H. Tzehoval, M. Steinberg, Appl. Surf. Sci. 17 (1983) 175.
[4] J. Soria, A. Martínez-Arias, J.C. Conesa, J. Chem. Soc., Faraday Trans. 91 (1995) 1669.
[5] M. Che, A.J. Tench, Adv. Catal. 32 (1983) 1.
[6] C. Binet, M. Daturi, J.-C. Lavalley, Catal. Today 50 (1999) 207.
[7] V.V. Pushkarev, V.I. Kovalchuk, J.L. d'Itri, J. Phys. Chem. B 108 (2004) 5341.
[8] J.C. Conesa, Surf. Sci. 339 (1995) 337.
[9] H. Nörenberg, G.A.D. Briggs, Surf. Sci. 424 (1999) L352.
[10] Y. Namai, K.-I. Fukui, Y. Iwasawa, J. Phys. Chem. B 107 (2003) 11666.
[11] F. Esch, S. Fabris, L. Zhou, T. Montini, C. Africh, P. Fornasiero, G. Comelli, R. Rosei, Science 29 (2005) 5735.
[12] J.-L. Lu, H.-J. Gao, S. Shaikhutdinov, H.-J. Freund, Surf. Sci. 600 (2006) 5004.
[13] S. Gritschneder, M. Reichling, Nanotechnology 18 (2007) 044024.
[14] M.V. Ganduglia-Pirovano, A. Hofmann, J. Sauer, Surf. Sci. Rep. 62 (2007) 219.
[15] B. Herschend, M. Baudin, K. Hermansson, Surf. Sci. 599 (2005) 173.
[16] B. Herschend, M. Baudin, K. Hermansson, J. Chem. Phys. 126 (2007) 234706.
[17] C. Müller, C. Freysoldt, M. Baudin, K. Hermansson, Chem. Phys. 318 (2005) 180.
[18] N.V. Skorodumova, S.I. Simak, B.I. Lundqvist, I.A. Abrikosov, B. Johansson, Phys. Rev. Lett. 89 (2002) 166601.
[19] Z. Yang, T.K. Woo, M. Baudin, K. Hermansson, J. Chem. Phys. 120 (2004) 7741.
[20] S. Fabris, S. de Gironcoli, S. Baroni, G. Vicario, G. Balducci, Phys. Rev. B 71 (2005), 041102(R).
[21] G. Kresse, P. Blaha, J.L.F. Da Silva, M. Veronica Ganduglia-Pirovano, Phys. Rev. B 72 (2005) 237101.
[22] S. Fabris, S. de Gironcoli, S. Baroni, G. Vicario, G. Balducci, Phys. Rev. B 72 (2005) 237102.
[23] J.L.F. Da Silva, M.V. Ganduglia-Pirovano, J. Sauer, V. Bayer, G. Kresse, Phys. Rev. B 75 (2007) 045121.
[24] P.J. Hay, R.L. Martin, J. Uddin, G.E. Scuseria, J. Chem. Phys. 125 (2006) 034712.
[25] S. Fabris, G. Vicario, G. Balducci, S. de Gironcoli, S. Baroni, J. Phys. Chem. B 109 (2005) 22860.
[26] M. Nolan, S. Grigoleit, D.C. Sayle, S.C. Parker, G.W. Watson, Surf. Sci. 576 (2005) 217.
[27] D.A. Andersson, S.I. Simak, B. Johansson, I.A. Abrikosov, N.V. Skorodumova, Phys. Rev. B 75 (2007) 035109.
[28] M.B. Watkins, A.S. Foster, A.L. Shluger, J. Phys. Chem. C 111 (2007) 15337.
[29] A. Beste, D.R. Mullins, S.H. Overbury, R.J. Harrison, Surf. Sci. 602 (2008) 162.
[30] C.W.M. Castleton, J. Kullgren, K. Hermansson, J. Chem. Phys. 127 (2007) 244704.
[31] S.F. Li, H. Lu, P. Li, Z. Yang, Z.X. Guo, J. Chem. Phys. 128 (2008) 164718.
[32] C. Loschen, J. Carrasco, K.M. Neyman, F. Illas, Phys. Rev. B 75 (2007) 035115.
[33] L. Petit, A. Svane, Z. Szotek, W.M. Temmerman, Phys. Rev. B 72 (2005) 205118.
[34] A. Stroppa, G. Kresse, New J. Phys. 10 (2008) 063020.
[35] A. Walsh, J.L.F. Da Silva, S.-H. Wei, Phys. Rev. Lett. 100 (2008) 256401.
[36] S. Kumar, P.K. Schelling, J. Chem. Phys. 125 (2006) 204704.
[37] N.V. Skorodumova, M. Baudin, K. Hermansson, Phys. Rev. B 69 (2004), 075401.
[38] N. Ichikawa, S. Sato, R. Takahashi, T. Sodesawa, H. Fujita, T. Atoguchi, A. Shiga, J. Catal. 239 (2006) 13.
[39] V. Shapovalov, H. Metiu, J. Catal. 245 (2007) 205.
[40] G. Kresse, J. Hafner, Phys. Rev. B 47 (1993) R558.
[41] G. Kresse, J. Hafner, Phys. Rev. B 49 (1994) 14251.
[42] G. Kresse, J. Furthmüller, Comput. Mater. Sci. 6 (1996) 15.
[43] G. Kresse, J. Furthmüller, Phys. Rev. B 54 (1996) 11169.
[44] P.E. Blöchl, Phys. Rev. B 50 (1994) 17953.
[45] G. Kresse, D. Joubert, Phys. Rev. B 59 (1999) 1758, All PAW potentials used, from the VASP library, are obtained by the method explained in this reference.
[46] J.P. Perdew, K. Burke, M. Ernzerhof, Phys. Rev. Lett. 77 (1996) 3865; J.P. Perdew, K. Burke, M. Ernzerhof, Phys. Rev. Lett. 78 (1997) 1396.
[47] S.L. Dudarev, G.A. Botton, S.Y. Savrasov, C.J. Humphreys, A.P. Sutton, Phys. Rev. B 57 (1998) 1505.
[48] M. Huang, S. Fabris, J. Phys. Chem. C 112 (2008) 8643.
[49] J. Zhang, R.B. von Dreele, L. Eyring, J. Solid State Chem. 104 (1993) 21.
[50] H.L. Tuller, A.S. Nowick, J. Phys. Chem. Solids 38 (1977) 859.
[51] E. Wuilloud, B. Delley, W.-D. Schneider, Y. Baier, Phys. Rev. Lett. 53 (1984) 202.
[52] J.C. Conesa, J. Phys. Chem. B 107 (2003) 8840.
[53] M. Huang, S. Fabris, Phys. Rev. B 75 (2007) 081404.
[54] X. Zhang, K.J. Klabunde, Inorg. Chem. 31 (1992) 1706.